Journal of Current Science and Technology, May-August 2023 Vol. 13 No. 2, pp. 182-204

ISSN 2630-0656 (Online)

Cite this article: Rajesh, P., Shajin, F. H., Ansal, V., & Kumar, B. V., (2023, May). Enhanced artificial transgender longicorn algorithm &recurrent neural network based enhanced DC-DC converter for torque ripple minimization of BLDC motor. *Journal of Current Science and Technology, 13*(2), 182-204. https://doi.org/10.59796/jcst.V13N2.2023.1735

Journal of Current Science and Technology

Journal homepage: https://jcst.rsu.ac.th

Enhanced artificial transgender longicorn algorithm &recurrent neural network based enhanced DC-DC converter for torque ripple minimization of BLDC motor

P. Rajesh[1*], Francis H Shajin[2], V. Ansal[3], and Vijay Kumar B[4]

[1*]Department of Electrical and Electronics Engineering, Anna University, Tamil Nadu, 600025, India
[2]Department of Electronics and Communication Engineering, Anna University, Tamil Nadu, 600025, India
[3]Department of Electrical and Electronics Engineering, NIT Goa, Goa,403401 India
[4]Department of Electrical and Electronics Engineering, Kakatiya Institute of Technology & Science, Warangal, 506015, India

*Corresponding author; E-mail: rajeshkannan.mt@gmail.com

Received 9 May 2022; Revised 30 August 2022; Accepted 16 September 2022;
Published online 15 July 2023

Abstract

This paper proposes an enhanced DC-DC converter with hybrid control method for torque ripple minimization of BLDC motor. Initially, a BLDC motor is controlled with an enhanced Cuk converter. The application of a switched inductor is used to update the Cuk converter operation. In this method, the control mechanism incorporates two control loops, namely, the speed control loop and torque control loop, which are utilized to recover the execution of BLDC. Thus, the proposed system is the combined performance of the Enhanced Artificial Transgender Longicorn Algorithm (EATLA) and Recurrent Neural Network (RNN) to improve control loop operations. In the Artificial Transgender Longicorn Algorithm (ATLA), the crossover and mutation approach are used as part of the scattering process to build the accuracy search process. In this article, the EATLA-RNN algorithm for limiting speed and torque error of BLDC motor is explored. However, the proposed method output is subject to input of the speed and torque controllers. The proposed topology with the controller is executed on MATLAB/Simulink workstation, and torque ripple minimization is analyzed toother existing approaches such as particle swarm optimization (PSO) and bacterial foraging (BF) algorithm.

Keywords**:** *BLDC; Cuk converter; EATLA; PSO; RNN; speed and current; torque ripples.*

1. Introduction

Nowadays, there is an increasing trend to use BLDC motors based on brushed DC (BDC) motors. BLDC motors have advantages i) better speed ii) increased dynamic response, iii) increased competition-long life iv) quiet operation and v) maximum speed range. Furthermore, the usage of BLDC motors has increased rapidly due to their high torque and power density, low manufacturing cost, high performance, and high-speed operation. They are extensively used in automotive, medical, and electronic applications, as well as in fans, compressors, and blowers (Singh, & Singh, 2012; Faiz, Nejadi-Koti, & Valipour, 2017; Shajin, Rajesh, & Raja, 2022). Brushless DC motors have not experienced the "slip" typically found on induction motors (Aghili, 2010; Rajesh, Shajin, & Cherukupalli, 2021). Typically, a simple BLDC motor takes a permanent magnetic rotor and 3 stator coils (Park, Park, Lee, & Harashima, 2000; Rajesh, Shajin, & Vijaya Anand, 2021).

Speed reflection has large overshoots at unstable intervals and large fluctuations at constant intervals (Aghili, Buehler, & Hollerbach, 2003; Seol, Kang, Jun, Lim, & Lee, 2017; Shajin, & Rajesh, 2022). The BLDC motor dual circuit speed control system is widely utilized in household and office automation (Kumar, & Singh, 2017; Fang, Li, & Han, 2011). Thus, suppressing commutation torque ripple is significant to diminish the BLDC motor torque (Ibrahim, Hassan, & Shomer, 2014). The system consists of cogging and reluctance torques; the mutual torque is induced through stator slots interacting with the rotor magnetic field (Niapour, Tabarraie, & Feyzi, 2014; Guzman, Duran, Barrero, Bogado, & Toral, 2013; Masmoudi, El Badsi, & Masmoudi, 2014; Sheng, Wang, Zhang, & Deng, 2014). Moreover, the reluctance torque is produced by the variation of the phase inductance relative to rotor position (Shi, Guo, Song, & Xia, 2009; Periasamy, & Umaya, 2018). Thus, an efficient controller is essential to decrease the harmonics on input voltage, as well as to minimize variations in line current pulse to the motor.

BLDC motor controller design consists of difficult processes such as modeling, control unit selection, simulation with parameter tuning (Lu, Zhang, & Qu, 2008). Various models, such as the phase shift superposition model and the pulse width modulation model, are recommended to overcome torque ripple. Various models, such as the phase shift superposition model and the pulse width modulation model, are recommended to overcome torque ripple.

Rotor speed, together with position information is essential for BLDC control approaches. Here, either sensors are used for measuring speed and position, or a few assessment strategies are employed to determine speed and position (Zhu, Zeng, & Zhao, 2016). The proportional integral (PI) based speed controller is induced into the BLDC motor.

At first, the BDC motor control is performed with enhanced Cuk converter. The operation of Cuk converter is updated using a switched inductor application. Thus, the proposed system is a joint implementation of Enhanced Artificial Transgender Longicorn Algorithm (EATLA) and a Recurrent Neural Network (RNN). The remaining document is structured as follows: Section 2 presents a review of the literature and its issues. Section 3 presents the proposed converter-based BLDC motor. Section 4 provides simulation outcomes and discussion. Section 5 provides the conclusion of the paper.

1.1 Literature survey

Several research studies have previously been published in the literature on BLDC motor torque ripple reduction, each utilizing different procedures and aspects. Here, some of these works are reviewed. Shi, Cao, Jiang, Li, and Xia (2017) revealed the feedback reward method in combination with sensored BLDC or a sensorless drive system to alter the switching timing by constraining the two-half-time current integrals over a 60-degree lead period. Singh et al., (2015) introduced power factor in terms of bridgeless Luo powered BLDC converter. Kumar, and Singh (2017) have deliberated on driving the BLDC motor with PV energy for water pump. The Cuk DC-DC converter was used in a solar photovoltaic cluster (SPV) at dangerous power. The starting current of the BLDC motor was controlled for optimal settings and for the determination of control parameters.

Jiang, Huang, Wang, Gao, & Wang (2016) have proposed a new control system for BLDC under compressive loading. Chen, Liu, Li, Shi, and Xia (2016) found an innovative commutation system for BLDCM. The control systems were applied to a two-phase standard structure using the Clark transformation, with the aim to shift time.

Chen et al., (2016) have introduced novel commutation torque ripple reduction technique for BLDCM in terms of Cuk converter. Ge, Zhu, Kemp, Moule, & Williams (2016) have suggested the conventional stepped pitch system for gear torque reduction in IPM machines. Bist, & Singh (2015) have introduced the stepped pitch rotor at optimal pitch angles, together with the stepped pitch rotor at unequal pitch lengths. Here, two improved systems were used to compensate for the three-dimensional effect and diminish the residual torque of the gear.

Çelikel, & Aydoğmuş (2019) have introduced an effective scheme to lessen torque ripple through wide speed control of BLDC motor. Initially, the conventional system with constant DC link voltage is implemented. Next, variable DC link was done with boost DC-DC. Thirdly, variable DC link voltage by boost-buck converter with PWM was realized. Çelikel, Özdemir, &

Aydoğmuş (2017) have implemented a present reference system which was applied to protect the current spikes from the solar power system. The PI controller was designed using Genetic Algorithms (Gas). Çelikel, & Özdemir (2019) have presented the CRM system to keep satellite power system as well as solar panels. The block diagram of the CRM system was used to control BLDC current.

Senthilnathan, & Palanivel (2020) have presented the comparatively simple control system resultant mostly from Outgoing Current Discharge Hysteresis Control (OCDHC). For digital controller performance, choose the Xilinx Spartan 6 FPGA board. Park, & Lee (2020) have presented the combination of a two-phase and a three-phase switching system to lessen the switching loss. At conduction region, the conventional two-phase switching topology was applied to decrease switching losses. An appropriate PWM duty ratio was determined to control current slope. Li, Kong, Cheng, & Liu (2020) have presented this torque ripple, driving control method alternates between two and three phase mode. The 3-phase conduction mode represents the rate of change of current with switching interval condensed competently, in the unswitched phase leftovers constant. Nithin, Vivek, & Purushothaman, (2020) have introduced switching mode selection circuit which has additional switch as well as diode with switching interval provide maximum voltage. This system was properly reduced torque ripple through switching at entire speeds, resulting at simpler modulator design. Patel, & Chandwani (2021) have presented BLDC motor through sinusoidal currents lessen voltage necessary to perform phase inductance based on quasi-square currents based on its shape. The closed loop control was attained by providing the PI controller speed control loop.

Kommula, & Kota (2022) have realized the DC-DC converter structure using hybrid control algorithm. At first, the BLDC motor modeling was designed through an improved Cuk converter. Sadda, Keshri, Tiwari, & Jain (2022) have explained a technique to decrease the torque ripples by closed loop isolated DC-DC buck-boost converter. PI controller was used at feedback to create a closed loop. With the fly back converter. Çorapsız, & Kahveci (2022) have presented a comparative analysis of Buck-Boost and SEPIC (Single Ended Primary Inductance) utilized. It was accepted at numerous studies to decrease torque ripples. Though BLDCM consists of numerous benefits, fluctuations in generated torque. BLDCM was investigated mathematically and problem causing switching torque waves was described.

1.2 Background of Research Work

Torque ripples are caused by electronic power switching, and maximum frequency use of power devices, and stator failure. Furthermore, the input supply voltage has various harmonic components, the pulsed input current and the switching phase currents causing torque ripple. Though, numerous systems have been executed to diminish torque ripple, like SVPWM, non-sinusoidal inverse EMF, etc. The BLDC motor should be supplied with restricted high power; in general, a large amount of heat can weaken the magnets and damage the winding protection. Since the motor rotor is a magnet, after the magnetization, a high magnetic field can alter the rotor's magnetic properties. An optimal torque control system using the best method is essential to solve this challenge. Therefore, the manuscript of the enhanced control system has been recognized to address the previous issues.

2. Objectives and Contribution

(a) An enhanced DC-DC converter configuration by hybrid control for BLDC motor torque ripple minimization. The proposed hybrid system combines the Enhanced Artificial Transgender Longicorn Algorithm (EATLA) and Recurrent Neural Networks (RNN). Initially, the outline of proposed system configuration is modeled. The optimal parameters are determined to optimize the controller operation update using the aid of necessary objective functions. The proposed system's performance is evaluated on the MATLAB/Simulink platform by comparing it with existing systems.

(b) The proposed optimization consists of two key functions. The initial function of the proposed system is accomplished by EATLA. The error signal goes with the proposed speed controller to control the speed by generating torque reference signals.

(c) The second function is achieved with RNN. Once the process is finished the hybrid technique can provide yield the minimum error factors.

3. Methodology

3.1 Proposed Converter depend on BLDC motor

Figure 1 illustrates the dynamic drive system of BLDC motor. This system includes BLDC motor, Voltage Source Inverter (VSI), DC filter, diode bridge rectifier (DBR) as well as AC voltage. BLDC motor is connected using VSI at 3 phase a, b, c, back EMF identified e^a, e^b, e^c.

The modeling part of BLDC is discussed Phase I. Initially, the AC input is delivered by DBR circuit. Depending on VSI, the BLDC engine optimally controls and examines its performances. Regarding that, in the paper, EATLA-RNN is proposed for controlling speed and torque should be improved. This process is identified from phase II process.

3.1.1 Phase-I: Modeling Method

Figure 2 illustrates the modeling part of BLDC using an equivalent circuit. It experiences maximum switching loss in solid-state switches of the voltage source inverter. The ordinary AC supply is provided as input and then switched to a DC supply. The enhanced operation of the Cuk converter is performed. Generally, the VSI and DC filter operating principles are previously known and mentioned in the document (Foroozeshfar, Adib, & Farzanehfard, 2014; Poorali, Adib, & Farzanehfard, 2017). The structure and operating performance of the improved Cuk converter are detailed as follows,

1) Enhanced Cuk Converter

A non-isolated improved Cuk has two components: (i) a switch and (ii) a diode. This results in a voltage that is negative relative to the input voltage (Esmaili, & Babazadeh, 2020). The switched inductor includes a switch and a steering diode (Shi, Niu, Chen, & Xia, 2017), which is shown on Figure 3.

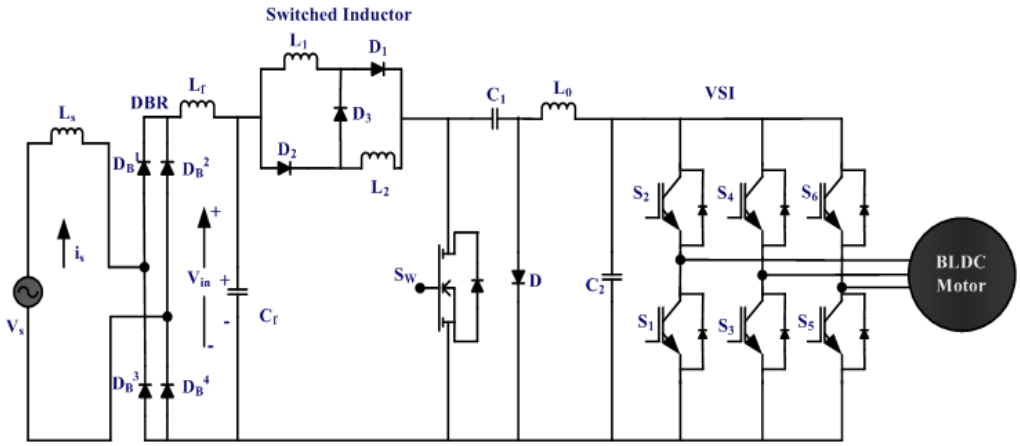

Figure 1 Organization of Cuk with BLDC

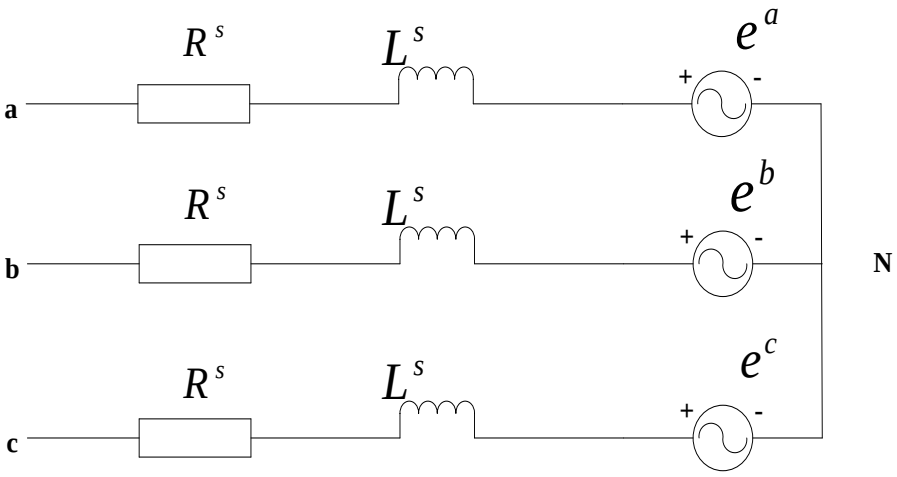

Figure 2 Equivalent circuit of every motor phase

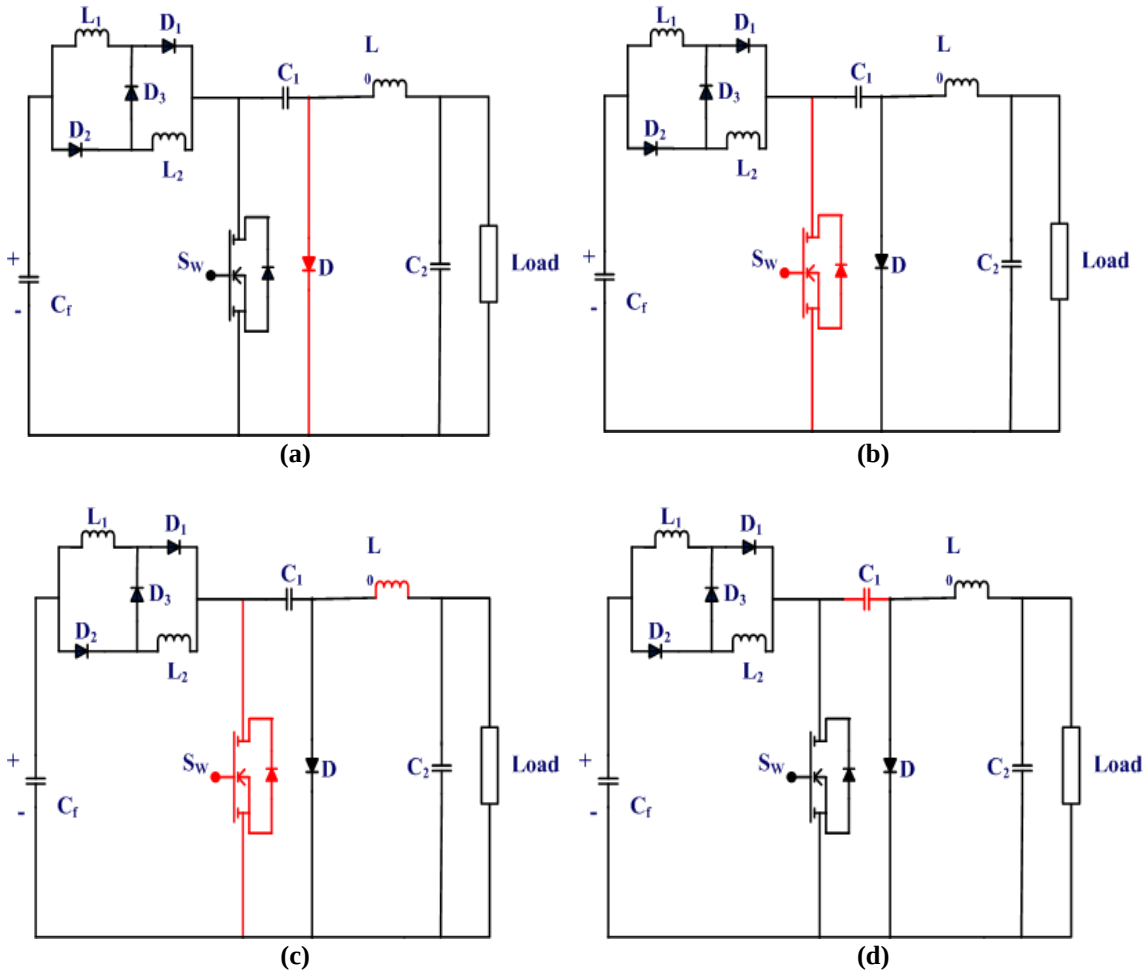

Figure 3 Operation of Enhanced Cuk converter on CCM (a, b), DICM (c, d) DCVM

When operating the actual switch platform, the two inductors are charged at parallel to the same power level. The current is controlled with parasite resistance, thus causing great vitality misfortune. Figure 3 (a, b) shows Cuk converter in CCM mode at 2 dissimilar switching intervals. In DICM together with operation of DCVM is demonstrated at Figure 3 (c and d).

At CCM the performance of current at switched inductor (L_1 and L_0) and voltage through middle of capacitance C_1 remain in switching period (Jiang et al., 2017). At mode 1, switch (*Sw*) specifies turned ON, when capacitance (C_1) is discharged during switch (*Sw*).

2) BLDC motor

Here, BLDC motor speed as well as torque controls (Çelikel, & Aydoğmuş, 2019; Çelikel, Reşat, Özdemir, & Aydoğmuş, 2017). Figure 2 portrays equivalent circuit of BLDC motor of every phase has been separately.

BLDC motor collected up to associated voltage condition (1).

$$\delta_{abc}^{s} = \frac{d}{dt}.\left(FL_{abc}^{s}\right) + \gamma^{s}.\psi_{abc}^{s} \tag{1}$$

Here γ^s refers stator resistance, δ refers stator voltage, ψ implies stator current, *FL* refers flux linkage and variables as $F_{abc}{}^{s}=[F_{ab}.F_{bc}.F_{cs}]^{T}$. Stator resistance array computed in equation (2).

$$\gamma^{s} = diag\left[\gamma^{s},\gamma^{s},\gamma^{s}\right] \tag{2}$$

The electromagnetic torque generated back-EMF harmonics is considered as associated condition (3).

$$\eta^{e} = \sum_{n=`1}^{\infty}(2n-1).k_{2n-1}.\begin{bmatrix}\psi_a^s\\ \psi_b^s\\ \psi_c^s\end{bmatrix}.\begin{bmatrix}cos(\theta^{\gamma}.(2n-1))\\ cos\left((2n-1).\left(\theta^{\gamma}-\frac{2x}{3}\right)\right)\\ cos\left((2n-1).\left(\theta^{\gamma}+\frac{2x}{3}\right)\right)\end{bmatrix}.\left(\frac{q}{2}.fl_m'\right) \tag{3}$$

where η^{e} refers electromagnetic torque in the presence of back-EMF.

$$e_{abc}^{s}=\sum_{n=`1}^{\infty}(2n\text{-}1).k_{2n\text{-}1}.\begin{bmatrix}\cos(\theta^{\gamma}.(2n\text{-}1))\\ \cos\left((2n\text{-}1).\left(\theta^{\gamma}-\frac{2x}{3}\right)\right)\\ \cos\left((2n\text{-}1).\left(\theta^{\gamma}+\frac{2x}{3}\right)\right)\end{bmatrix}.(\omega^{\gamma}.fl_m') \tag{4}$$

$$\frac{d}{dt}.(\varphi^{\gamma}) = \left(\frac{P}{2j}\right)..(\eta^{e}-\eta^{m}) \tag{5}$$

Where ${}^{d}_{dt}.(\chi^{\gamma})$ represents the electrical angular speed of rotor, η^m refers joint mechanic. Here, the torque waves and speed analysis of the BLDC motor. Similarly, torque is evaluated as controller. The BLDC motor strategy is identified at next section.

3.1.2 Phase-II: Control Process

This paper suggests the new topology and control method based on the EATLA-RNN system. Figure 4 represents the control structure of the proposed system. The PI controller based on the proposed method is created to control the speed. The signals are transmitted with the VSI, it should generate optimum pulses to regulate the BLDC motor. With respect to the three phase source voltage (V_{sa},V_{sb} *and* V_{sc}) is given to the input.

(i) Speed controller

In BLDC motor, the speed assesses with speed evaluator. The speed error resolute its real and reference value. The PI controller enhancement is based on parameters K_p, Ki.

$$U = K_p e_s(t) + K_i \int e_s(t)dt \tag{6}$$

In the same way, the output signal provides the EATLA-RNN technique. At operation of EATLA RNN method, the ATLA system is executed, which is updated by crossover and mutation method. From this output of the proposed algorithm, the corresponding gains parameter values.

$$\xi(U) = K_p^{'} e_s(t) + K_i^{'} \int e_s(t)dt \tag{7}$$

(ii) Torque control

The torque error values are specified as PI controller to obtain the optimal control pulses.

$$\xi(\Delta) = K_p^{''} e_t(t) + K_i^{''} \int e_t(t)dt$$

Here

$$\Re\rho = \frac{T_{max\,x} - T_{min}}{T_{max\,x} + T_{min}} \tag{8}$$

The optimal growth of control signals is expressed mathematically at below equation (9).

$$D(t) = \begin{cases} if\ e(t) > TD; & then\ D(t) = T_{on}^{\max} \\ if\ e(t) < TD; & then\ D(t) = T_{off}^{\max} \end{cases} \quad (9)$$

Here TD refers threshold value; T_{on} and T_{off} refers on and off period. The next section denotes that comprehensive working procedures of proposed system.

3.2 Torque Ripple Minimization of BLDC by Hybrid Technique

The proposed hybrid system involved for torque ripple minimization of BLDC motor is Enhanced Artificial Transgender Longicorn Algorithm (EATLA) & recurrent neural networks (RNN) are suggested to improve the control loop functions.

3.2.1 Proposed Techniques

1) Mathematical Representation of Enhanced Artificial Transgender longicorn Algorithm (EATLA)

The algorithm of ATLA is based on two phases, which are also called Heterosexual attraction and random search movement phases. The main aim of the ATLA is briefly elaborated below (Han, Du, & Yu, 2020). The EATLA method realistically achieves the optimal mean error value. At first, the error signals are initialized, and PI controller gain parameters are randomly created. For the initial population in applying EATLA, error values Ei are computed based on the variance between speed and torque values. To initialize the population, the longicorn form of the individuals in the group is classified as male. After completing the initialization and performing one random step, the male longicorn with the highest fitness, based on the fitness function, is chosen (Senthilnathan, & Palanivel, 2020).

To initialize the population of longicorn form the individuals in the group as a male gender.

$$Fitness = \min(E) \quad (10)$$

To attract the male longicorn and to mate, the transgender longicorn releases the sex pheromone. The male longicorn is exaggerated using the sex pheromone during the heterosexual attraction movement walks forward the female longicorn along with the concentration source direction is expressed as follows:

$$\vec{d}_i = \frac{X_{best}^t - X_i^t}{\left\| X_{best}^t - X_i^t \right\|}, i = 1,2,...,m \quad (11)$$

where the i-th male position is represent as X_i ; the current number of iteration is represented as 't' ; the position of the female longicorn with highest fitness under herd is mention as X_{best}; The male longicorn in the concentration range is denotes as 'm'. The male longicorn position is expressed as:

$$X_i^{t+1} = X_i^t + S_i^t \times \vec{d}_i \quad (12)$$

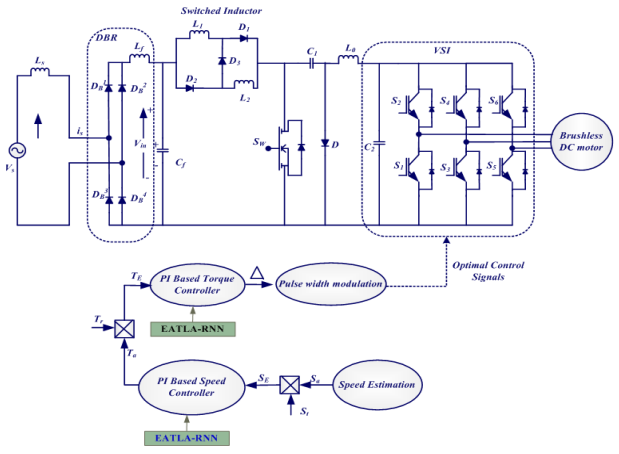

Figure 4 Control organization of Cuk converter depends on BLDC motor

The step size assigned from parameter not only to recover the search speed at initial phase, but also consider search precision at later phase of algorithm. The individual falling in to the local optimum is neglected by the step size, which decays the number of iterations shown in equation (13).

$$S_i^t = \frac{0.95S^{t-1}}{r_i} \tag{13}$$

While, the i-th male longicorn fitness ranking is denoted as r_i. If the male longicorn is not receiving the sex pheromone due to external concentration, the search takes place in a random manner. This random search is facilitated by the method of a levy flight, as described in equation (14).

$$X_i^{t+1} = X_i^t + \alpha \oplus L(\lambda), \quad i = 1,2,...,m \tag{14}$$

While "$\oplus$" is denoted as the point-to-point multiplication operator, $L(\lambda)$ defined as the random walk and its step size is expressed as 'u' which follows the Levy distribution, as shown in the following equation:

$$L(\lambda) \sim u = t^{-\lambda},\ 1 \le \lambda \le 3 \tag{15}$$

where λ is equal to 2.

Crossover: Among two longicorn crossovers rate is accomplished creates a novel set of longicorns. This process is done on the fitness value of longicorn and newly created longicorn.

Mutation: In view of specific rate of mutation under mutation process, longicorn mutate randomly.

For calculating crossover X_{over} and mutation Mu_{rate} rate of longicorn are computed depends on below equations.

$$X_{over} = \frac{N}{L} \tag{16}$$

$$Mu_{rate} = \frac{M}{L} \tag{17}$$

where N denotes number of longicorn crossover, M represents mutation and L refers length of longicorn.

The ATLA objective function is utilized to compute the fitness value for EA longicorn. The sex pheromone of female longicorn is received by male longicorn under the threshold range and moves towards it at same time that male longicorn present exterior the threshold range involves in random search. The threshold value is calculated using the fitness value by ranking. The male longicorn present under ranking range is influenced with the sex pheromone. To prove that the optimal value cannot be determined only under the threshold range of longicorn beetles, also herd of longicorns that falls into the local optimum is neglected by making the residual longicons. The maximal number of iterations is extended, the procedure exiting at that point; otherwise the mutation and crossover process is performed. The flow diagram of the ATLA algorithm portrays on Figure 5. Table 1 shows that pseudo code of the entire ATLA process.

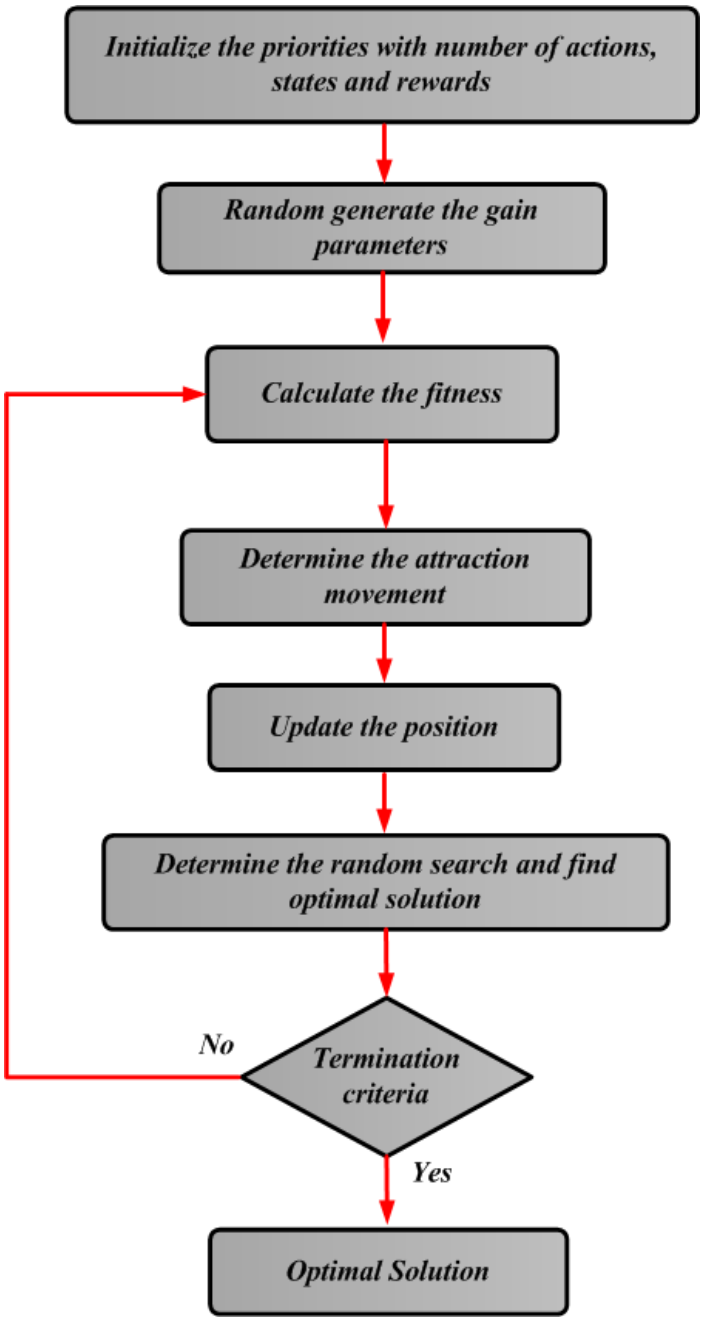

Figure 5 Flow chart of ATLA algorithm

Table 1 Pseudo code of ATLA algorithm

Algorithm: ATLA for overall minimal searching
Input: Create objective function $f(X^t)$, here $X^t = [X_1, X_2, ...X_n]^T$, .
Output: X_{best}, F_{best}.
If$(t < T) or (end\ criteria)$ do
Random lévy-fight of the entire longicorn;
Modify the better fitness female and discharge sex pheromones;
if X_i refers ranking range
Create their $\vec{d_i}$. and move with femina based on Equation (4);
else
Perform random search movement based on Equation (5);
Upgrade t;
End while
Return X_{best}. and , F_{best}.

2) Mathematical Representation of Recurrent Neural Network (RNN)

For learning and perception capabilities, the RNN is the most preferred control scheme, and the primary function of the RNN control scheme is interconnected with that of artificial neurons (Haddad Pajouh et al., 2018), (Transpire Online). The steps of the RNN controller are given as follows,

Steps of RNN.

Step 1: To train this proposed system, the input/output data is gathered. RNN is utilized to train the EATLA to mimic the training data presented to it, adjusting the parameters according to the selected error criterion.

$$\mathrm{A} = \{\mathrm{A}_1, \mathrm{A}_2, \mathrm{A}_3 \cdots \mathrm{A}_m\}^T \tag{18}$$

The hidden unit j specified by,

$$hidden_j^h = \sum_{i=1}^{m} z_{ji}\omega_i + \sigma_j^h \tag{19}$$

here z_{ji} denotes weight on connection as ith input unit.

Step 2: At hidden layer the neuron output is follow,

$$M_j^h = f\left(\sum_{i=1}^{m} z_{ji}\omega_i + \sigma_j^h\right) \tag{20}$$

$$hidden_k^o = \sum_{j=1}^{m_h} z_{ji}\omega_i + \sigma_j^o \tag{21}$$

Step 3: At last, neurons output is formulated with below equation,

$$\mathrm{O}_k^o = f\left(\sum_{j=1}^{m_h} z_{ji}\omega_i + \sigma_j^o\right) \tag{22}$$

Step 4: Fitness function is assessed using accompanying equation,

$$F = Min(E) = Min\{V_{dc}^{ref} - V_{dc}^{act}\} \tag{23}$$

here shunt APF; E refers error value among dc link voltage V_{dc}^{ref} and real dc link voltage as V_{dc}^{act} .

Step 5: The error is assessed from equation (24)

$$\Delta E = E(t) - E(t-1) \tag{24}$$

Step 6: Synaptic weights for upgrading terminologies provided below,

$$z_{ji}(n+1) = z_{ji}(n) - \xi\left(\frac{\partial MSE}{\partial z_{ji}(n)}\right) + \beta\Delta z_{ji}(n) \tag{25}$$

$$\Delta z_{ji}(n) = z_{ji}(n) - z_{ji}(n-1) \tag{26}$$

here, the learning factor is denoted by ξ, and the momentum factor is denoted by β. Normally, the RNN structure is fitted using least squares estimation and the back-propagation algorithm. For a broad assortment of control applications, the RNN system can be used in perspective on its adaptability. The proposed controller is effective for progressively controlling the UPFC performance. The RNN is trained by providing the

vector input to the proposed control system. Based on the EATLA-RNN strategy, the proper output control pulses are provided to the voltage source inverter, which powers the BLDC motor supply. Consequently, the torque ripples are optimally controlled.

4. Result and discussion

The EATLA-RNN system is replicated using a BLDC motor and is implemented on the MATLAB/Simulink platform. It is implemented with a BLDC motor powered by a six-switch VSI. First, BLDC motor parameters such as stator EMF, stator current, speed, and torque are examined accordingly. According to speed controller output, an optimal reference torque signal is created. An EATLA-RNN operated on the torque controller delivers the optimal VSI control pulses for BLDC motor control.

Case 1: Steady state Analysis

Case 2: Dynamic state Analysis

a) Speed variation in the positive direction (700 to 1500 rpm)

b) Speed variation in both positive and negative directions (1000 to -1000 rpm)

c) Torque variant and Speed

Depending on the EATLA-RNN system, the performance of the BLDC motor is compared with different systems such as PSO, BF, and the basic model. The parameters for the BLDC and CUK converter are portrayed in Table 2.

Analysis of Case 1

This indicates the standard condition rating of the BLDC motor. Figure 6 shows a BLDC motor operating at a steady state of 1000 rpm. Figure 6 (a) and (b) portray the actual and reference speeds at 1000 (rpm). Figure 6 shows (c) BF and (d) normal.

Figure 7 illustrates the performance of both the proposed and existing systems. Sub frame 7 (a) shows the current output performance of the proposed system, with a rise time of 0 seconds and a settling time of 0.25 seconds. Sub frame 7 (b), (c), and (d) portray the existing systems, where 0 seconds signifies the start time, and the settling times are 0.3 seconds, 0.33 seconds, and 0.44 seconds, respectively. Figure 8 represents the performance assessment of the EMF output according to the EATLA-RNN methodology.

Table 2 BLDC and CUK converter

BLDC motor	
BLDC parameters	**Value**
Stator resistance Rs	0.2
Stator inductance Ls	8.5e-3
Flux	0.176
Back EMF flat	120
Inertia, viscous damping, static friction	[0.089,0.005,4]
CUK Converter	
Input	12V
Output	30V
Power rating	18W
Inductor L_1	560μH
Inductor L_2	2.86 mH
Capacitor C_1	2 μF
Capacitor C_2	470 μF

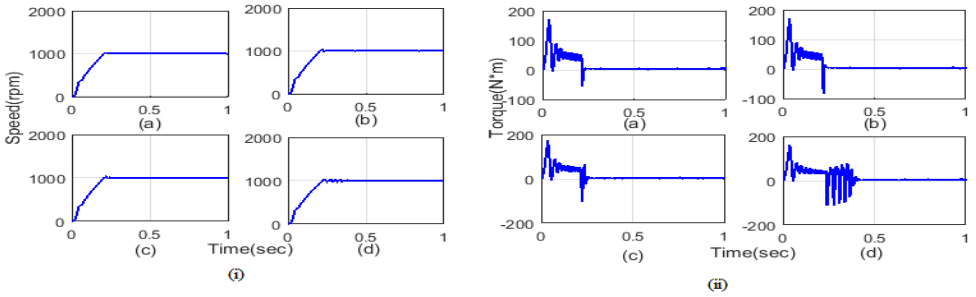

Figure 6 Performance of (i) Speed (ii) Torque with (a) EATLA-RNN system (b) particle swarm optimization (c) Bacterial Foraging (d) Usual System

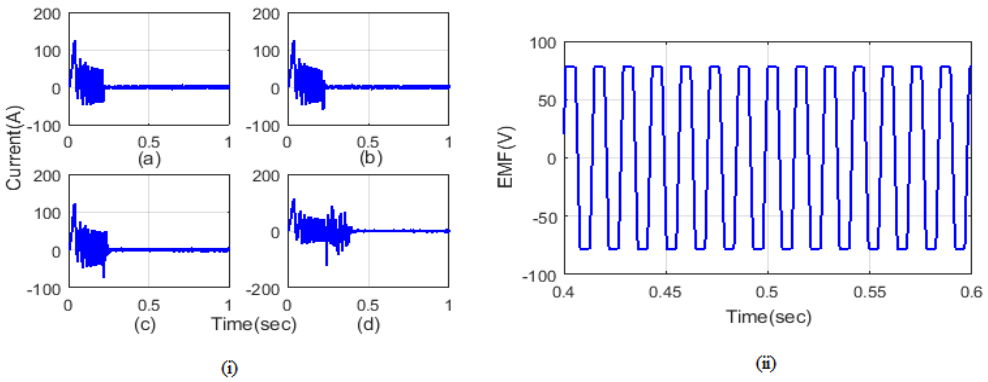

Figure 7 Performance of (i) current with (a) EATLA-RNN system (b) particle swarm optimization (c) Bacterial Foraging (d) Usual System (ii) EMF

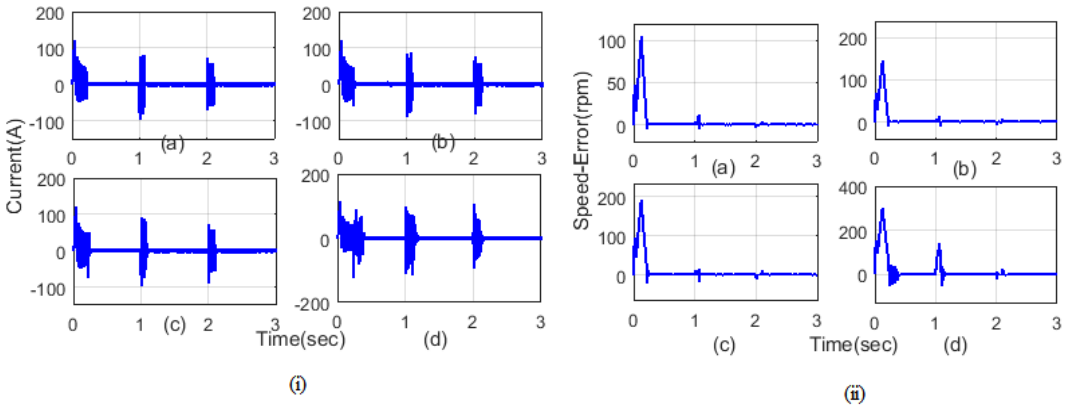

Figure 8 Performance of (i) Current (ii) Speed (a) EATLA-RNN (b) particle swarm optimization (c) Bacterial Foraging (d) Usual System

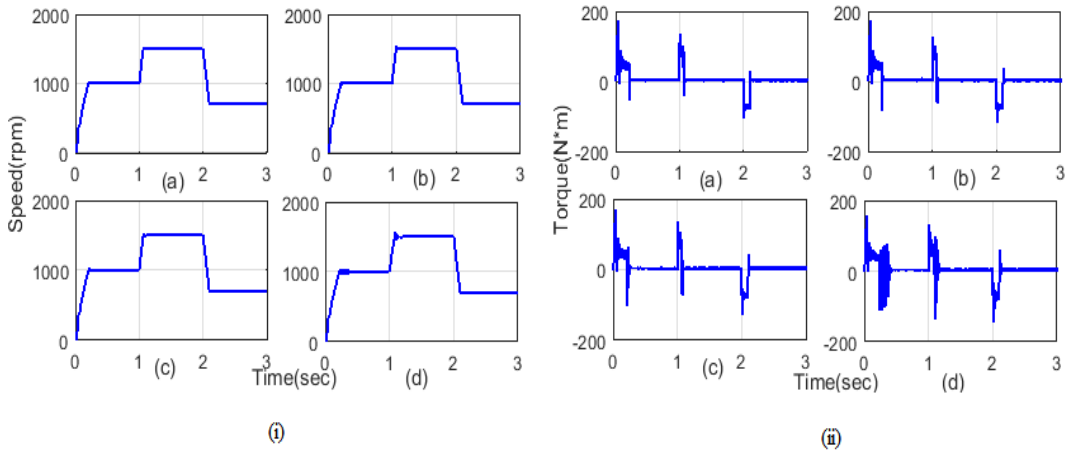

Figure 9 Performance of (i) Speed (ii) Torque (a) EATLA-RNN (b) particle swarm optimization (c) Bacterial Foraging (d) Usual System

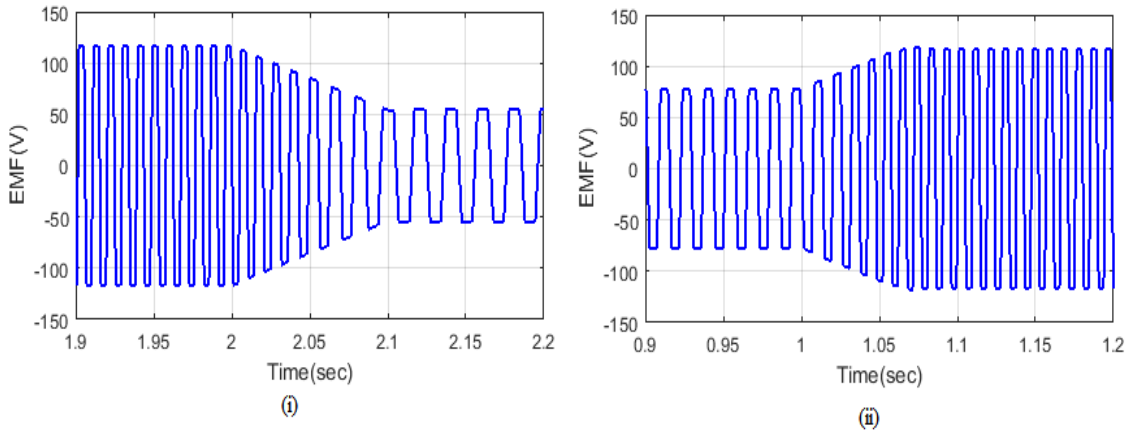

Figure 10 Performance of EMF with Speed Difference (i) 1500 – 700 (ii) 1000-1500

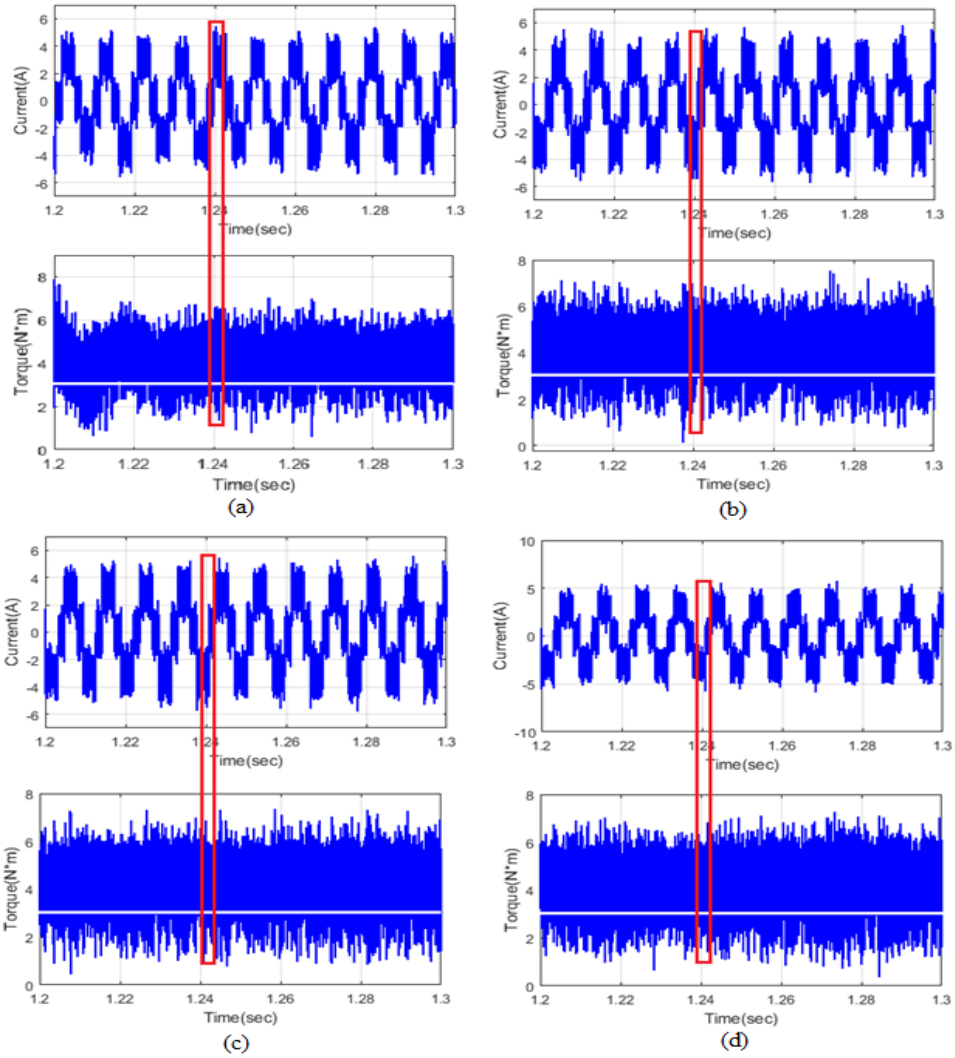

Figure 11 Torque with (a) Usual (b) PSO (c) BF (d) EATLA-RNN system

Case 2

Dynamic states are considered to investigate the BLDC motor, with three analysis states performed using both the proposed and existing systems.

Speed Variant at 700 to 1500 rpm

Figures 8 and 9 show the EATLA-RNN and the existing systems, where speed varies up to a high speed (i.e., 1500 rpm) from t = 1-2 seconds. These figures demonstrate variation according to time, focusing on a period from 0 to 3 seconds. The corresponding back electromotive force is also discussed in Figure 10. An equivalent torque is discussed on Figure 11 (a).

In the EATLA-RNN method, the torque ripple removal waveform is depicted in Figure 11(b). Figures 11(c and d) show current ripple output results; as a result, ripple output has been drastically reduced, with an average load torque value of 1.3 required to execute the PSO system.

Speed Variant on 1000 to -1000 rpm

Figures 12 and 13 display the simulated results, as well as the output of the EMF phase orientation under nominal speeds of 1000 and -1000 rpm.

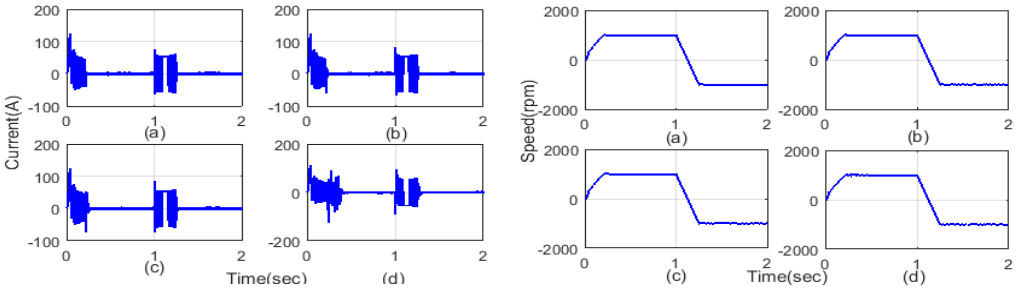

Figure 12 Performance of (i) Current (ii) Speed with (a) EATLA-RNN (b) particle swarm optimization (c) Bacterial Foraging (d) Usual System

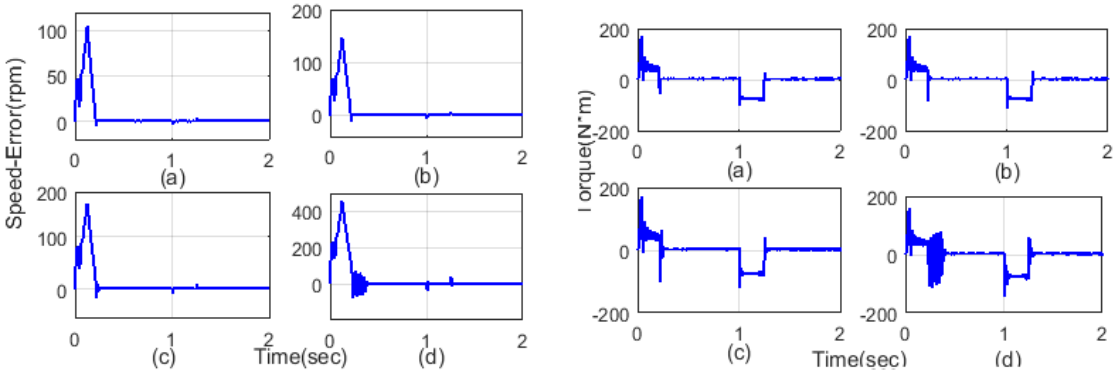

Figure 13 Performance of (i) Speed (ii) Torque (a) EATLA-RNN (b) particle swarm optimization (c) Bacterial Foraging (d) Usual System

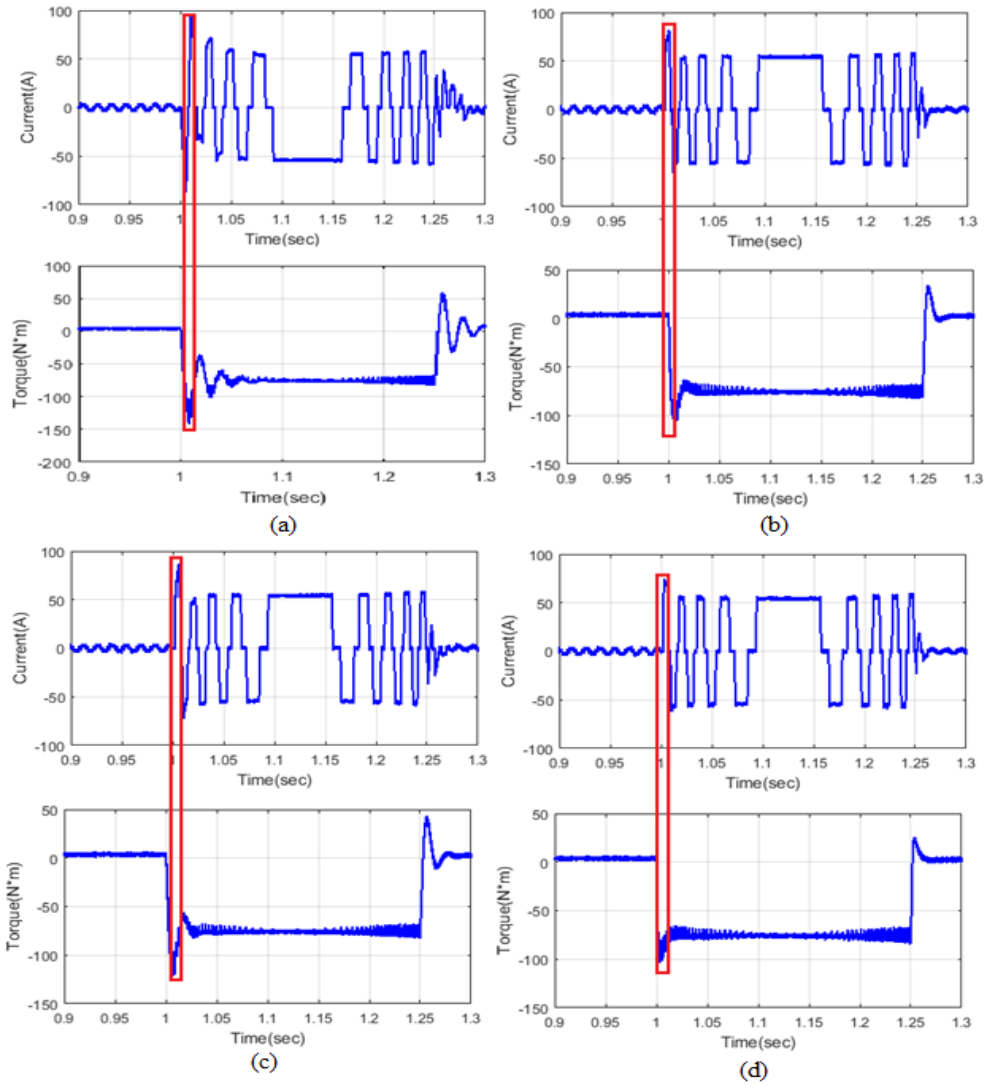

Figure 14 Torque ripple performancewith (a) Usual (b) particle swarm optimization (c) Bacterial Foraging (d) EATLA-RNN system

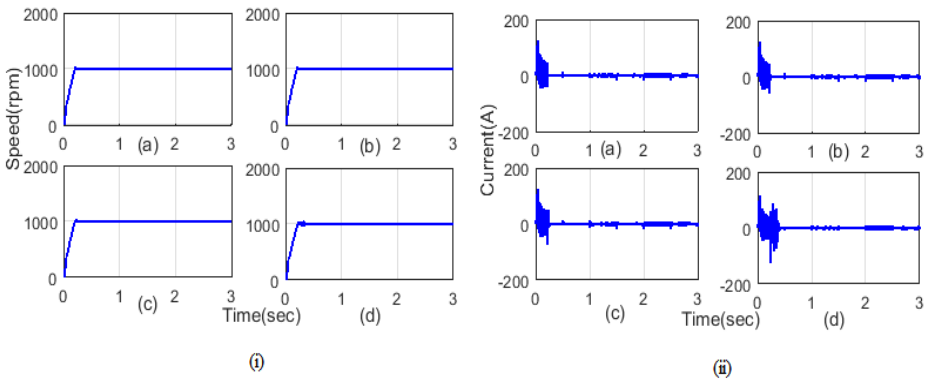

Figure 15 Performance of (i) Speed (ii) Current with (a) EATLA-RNN system (b) particle swarm optimization (c) Bacterial Foraging (d) Usual System

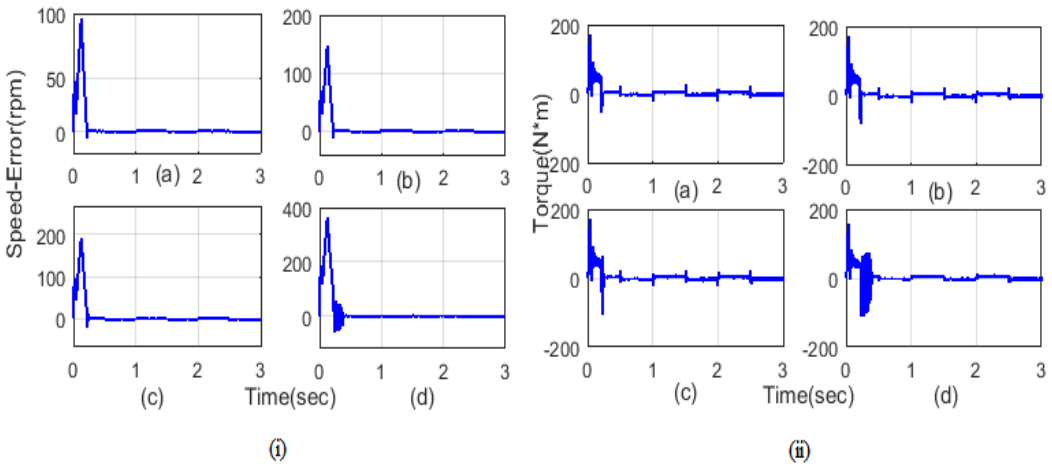

Figure 16 Performance of (i) Speed (ii) Torque (a) EATLA-RNN (b) particle swarm optimization (c) Bacterial Foraging (d) Usual System

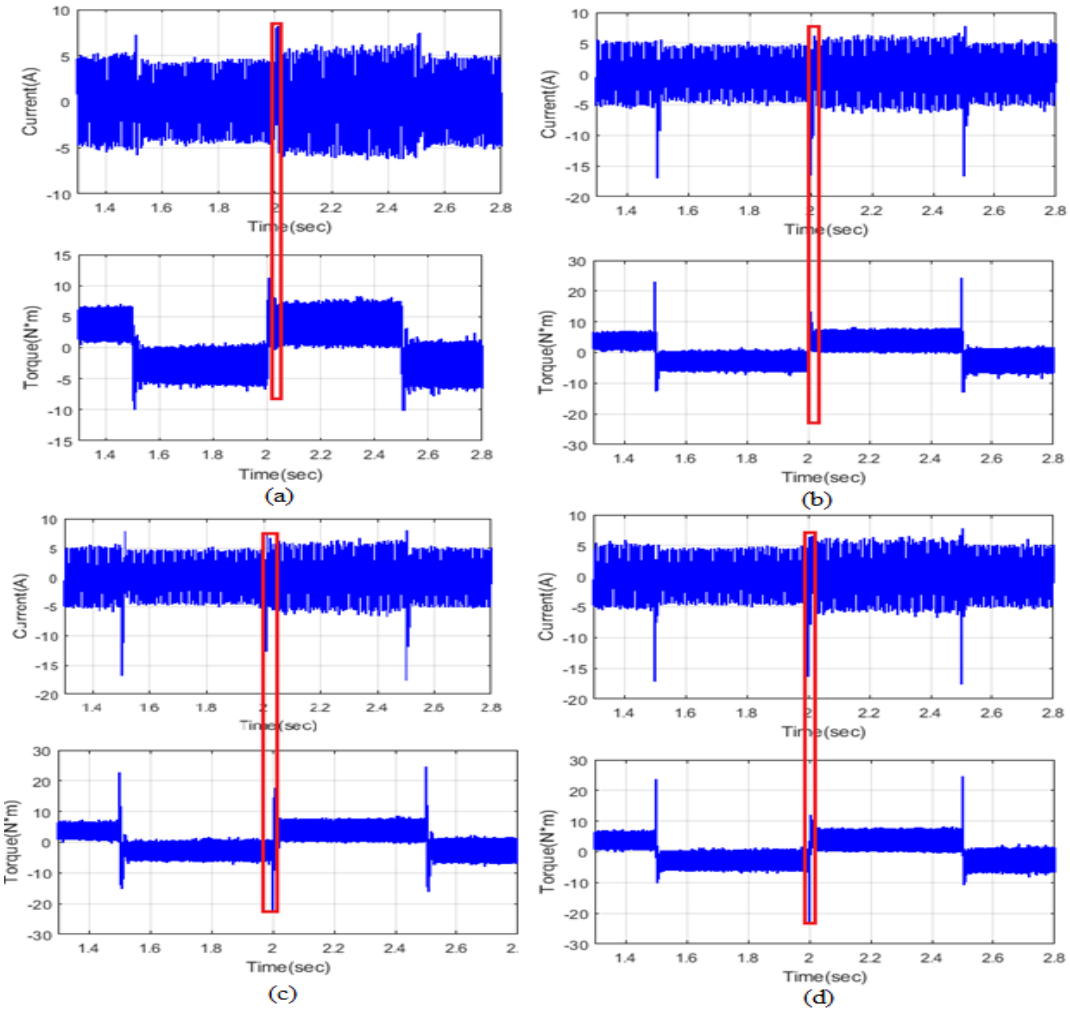

Figure 17 Torque ripples performance with (a) Usual (b) particle swarm optimization (c) Bacterial For aging (d) EATLA-RNN system

Figure 14 illustrates torque ripple with the established system compared to existing systems.

(C) Torque Variant on 3.3 to -3.3 and constant Speed

The EATLA-RNN system is based on minimizing the torque ripple in a BLDC motor. Figure 15 portrays a BLDC motor. The speed error process, relying on the PSO and BF technique, takes 150 (rpm) and 190 (rpm) respectively. Figure 16 (i) and (ii) depict velocity and current analyses respectively. The current output performance analysis of the established and previous systems is shown in Figure 16(ii).

Figure 17 (a, b, c, and d) illustrate the simulation results for current waveforms as well as electromagnetic torque comparisons between the EATLA-RNN system and existing systems, which correspondingly reduce switching torque.

Figure 17(a) illustrates the current ripple outcome of the BLDC motor, with the torque ripple being drastically decreased to a -2.5 load torque when implementing the PSO system. Figure 17(b) shows that the current output ripples have been drastically decreased to an average load torque value of -12. The EATLA-RNN system for removing high torque from the waveform is demonstrated in Figure 17(c). Figure 17(d) displays the current ripple of the motor torque ripple being drastically reduced to an average load torque value of -12 when employing the BF system.

Table 3 displays a comparison of EATLA-RNN with existing methodologies for different trials. At 50 trials, the EATLA-RNN method achieves an accuracy of 0.98, specificity of 0.97, recall of 1.61, and precision of 0.98. The PSO ranges achieve 0.69, 0.43, 0.14, and 0.39. The BF ranges achieve 0.73, 0.55, 0.37, and 0.66. Over 100 trials, the EATLA-RNN model attains an accuracy of 0.96, specificity of 0.93, recall of 0.87, and precision of 0.99. The PSO ranges achieve 0.55, 0.38, 0.66, and 0.65, while the BF ranges are 0.77, 0.57, 0.73, and 0.64. The experimental results validate that the EATLA-RNN system is more effective than existing systems.

4.1 Statistic Evaluation

Statistical measurements are used to calculate the error by root mean square error (RMSE), mean absolute percentage error (MAPE), and mean bias error (MBE).

Table 3 Performance of EATLA-RNN via existing approaches for different trials

Performance	50 trails		
	PSO	**BF**	**EATLA-RNN**
Precision	0.69	0.73	0.99
Specificity	0.43	0.55	0.97
Recall	0.14	0.37	1.59
Accuracy	0.40	0.66	0.98
100			
Precision	0.56	0.78	0.97
Specificity	0.40	0.58	0.94
Recall	0.67	0.73	0.88
Accuracy	0.65	0.64	0.98

Table 4 Comparison of EATLA-RNN using existing methodologies for dissimilar trials

Metrics	50 trails		
	PSO	**BF**	**Proposed**
RMSE	33.4	16.8	8.27
MAPE	18.6	9.6	0.96
MBE	893	7.2	1
100 trails			
RMSE	25.9	28.3	8.39
MAPE	13.8	5.7	2.92
MBE	18.8	8.7	3.88

Table 5 Power quality parameter frame as MSE and voltage deviation with numerous solution methods

Cases	MSE			Voltage deviation		
	PSO	BF	EATLA-RNN	PSO	BF	EATLA-RNN
Case 1	0.03041	0.28231	0.01093	8	10	5
Case 2	0.03040	0.04717	0.01095	15	10	5

Table 6 Framing of power factor using various solution techniques

Cases	Power factor		
	PSO	BF	Proposed
Case 1	25	70	50
Case 2	30	80	40

Table 7 Time response specifications of solution techniques

Specifications	Solution techniques		
	PSO	BF	Proposed
%Peak overshoot	538.51	524.7	**500.123**
Settling time (second)	2.9946	2.3745	**1.0179**

Table 8 Torque ripple minimization of solution methods

Torque ripple minimization (%)	Solution techniques		
	PSO	BF	Proposed
	36.7	22.36	**1.28**

When a large disturbance occurs at the target value, the mean square error value is high. If the MBE is negative, the diagnosis is prognostic. Table 4 displays the statistical performance of the EATLA-RNN technique. In Tables 5 and 6, the most desirable dataset encapsulates the maximum number of power quality parameters using the proposed technique. Table 5 presents the power quality frame parameters such as MSE and voltage deviation. The framing of the power factor using various solution techniques is given in Table 6. The power factor values for the proposed technique under case 1 are 50, and under case 2, they are 40. The time specifications for testing the dynamic performance of the proposed technique can also be found in Table 7. From these results, it is evident that the peak excess and settling time are reduced by the proposed system. The peak overshot (%) of the proposed system is 500.123, and the settling time (second) of the proposed method is 1.0179 seconds. Torque ripple minimization of solution systems is portrayed in Table 8.

5. Conclusion

In this article, the hybrid EATLA-RNN method is utilized to examine the dynamic behaviors of a BLDC motor. The brushless DC motor, dependent on the EATLA-RNN system, is implemented on a MATLAB/Simulink workstation. In the control component, the torque speed is regulated by the EATLA-RNN technique. As such, an enhanced proportionate integral controller is proposed to control the speed and reduce torque ripple of the BLDC motor system. The BLDC motor is tested under both steady and dynamic states. The efficiency of the EATLA-RNN system is analyzed in comparison with existing approaches such as the PSO and BF approach. Furthermore, the torque ripples are resolved using the EATLA-RNN method in conjunction with existing systems. Finally, the experimental outcomes indicate that the proposed EATLA-RNN system is effective compared to other existing systems. Therefore, the torque ripple can be reduced to almost half its value with the proposed controller model.

Data Availability Statement

Data sharing is not applicable to this article as no new data was created or analyzed.

Funding Information

This research did not receive any specific grants from funding agencies in the public, commercial, or non-profit sectors.

6. Acknowledgements

None

7. Reference

Aghili, F. (2010). Ripple suppression of BLDC motors with finite driver/amplifer bandwidth at high velocity. *IEEE transactions on control systems technology*, *19*(2), 391-397. https://doi.org/10.1109/TCST.2010.2045502

Aghili, F., Buehler, M., & Hollerbach, J. M. (2003). Experimental characterization and quadratic programming-based control of brushless-motors. *IEEE transactions on control systems technology*, *11*(1), 139-146. https://doi.org/10.1109/TCST.2002.806453

Bist, V., & Singh, B. (2015). Reduced sensor configuration of a power factor correction based single-ended primary inductance converter fed brushless DC motor drive. *IET Power Electronics*, *8*(9), 1606-1615. https://doi.org/10.1049/iet-pel.2014.0981

Çelikel, R., Özdemir, M., & Aydoğmuş, Ö. (2017). Implementation of a flywheel energy storage system for space applications. *Turkish Journal of Electrical Engineering and Computer Sciences*, *25*(2), 1197-1210. https://doi.org/10.3906/elk-1507-259

Çelikel, R., & Aydoğmuş, Ö. (2019) A torque ripple minimization method for brushless dc motor in high speed applications. *Journal of Engineering Research*, *7*(3), 200-214.

Çelikel, R., & Özdemir, M. (2019). A method for current control of the flywheel energy storage system used in satellites. *Tehničkivjesnik*, *26*(3), 631-638. https://doi.org/10.17559/TV-20160328090219

Chen, W., Liu, Y., Li, X., Shi, T., & Xia, C. (2016). A novel method of reducing commutation torque ripple for brushless DC motor based on Cuk converter. *IEEE Transactions on Power Electronics*, *32*(7), 5497-5508. https://doi.org/10.1109/TPEL.2016.2613126

Çorapsız, M. R., & Kahveci, H. (2022). Performance Analysis of Buck-Boost and SEPIC Converter for Commutation Torque Ripple Minimization in BLDC Motors. *Electric Power Components andSystems*, *49*(11-12), 1052-1067. https://doi.org/10.1080/15325008.2022.2049653

Esmaili, A., & Babazadeh, H. (2020). A foreground self-calibration technique for high-resolution switched current R-2R digital-to-analog converters. *Circuits, Systems, and Signal Processing*, *39*(5), 2307-2327. https://doi.org/10.1007/s00034-019-01284-x

Faiz, J., Nejadi-Koti, H., & Valipour, Z. (2017). Comprehensive review on inter-turn fault indexes in permanent magnet motors. *IET Electric Power Applications*, *11*(1), 142-156. https://doi.org/10.1049/iet-epa.2016.0196

Fang, J., Li, H., & Han, B. (2011). Torque ripple reduction in BLDC torque motor with nonideal back EMF. *IEEE transactions on power electronics*, *27*(11), 4630-4637. https://doi.org/10.1109/TPEL.2011.2176143

Foroozeshfar, R., Adib E., & Farzanehfard, H. (2014). New single-stage, single-switch, soft-switching three-phase SEPIC and Cuk-type power factor correction converters. *IET Power Electronics*, *7*(7), 1878-1885. https://doi.org/10.1049/iet-pel.2013.0443

Ge, X., Zhu, Z. Q., Kemp, G., Moule, D., & Williams, C. (2016). Optimal step-skew methods for cogging torque reduction accounting for three-dimensional effect of interior permanent magnet machines. *IEEE Transactions on Energy*

Conversion, *32*(1), 222-232. https://doi.org/10.1109/TEC.2016.2620476

Guzman, H., Duran, M. J., Barrero, F., Bogado, B., & Toral, S. (2013). Speed control of five-phase induction motors with integrated open-phase fault operation using model-based predictive current control techniques. *IEEE Transactions on Industrial Electronics*, *61*(9), 4474-4484. https://doi.org/10.1109/TIE.2013.2289882

Haddad Pajouh, H., Dehghantanha, A., Khayami, R., & Choo, K.K. (2018). A deep recurrent neural network based approach for internet of things malware threat hunting. *Future Generation Computer Systems*, *85*, 88-96. https://doi.org/10.1016/j.future.2018.03.007

Han, X., Du, X., & Yu, P. (2020). ATLA: A novel metaheuristic optimization algorithm inspired by the mating search behavior of longicorn beetles in the nature. *InIOP Conference Series: Materials Science and Engineering*, *782*(5),052028). IOP Publishing. https://doi.org/10.1088/1757-899X/782/5/052028

Ibrahim, H. E., Hassan, F. N., & Shomer, A. O. (2014). Optimal PID control of a brushless DC motor using PSO and BF techniques. *Ain Shams Engineering Journal*, *5*(2), 391-398. https://doi.org/10.1016/j.asej.2013.09.013

Jiang, G., Xia, C., Chen, W., Shi, T., Li, X., & Cao, Y. (2017). Commutation torque ripple suppression strategy for brushless DC motors with a novel noninductive boost front end. *IEEE Transactions on Power Electronics*, *33*(5), 4274-4284. https://doi.org/10.1109/TPEL.2017.2721439

Jiang, W., Huang, H., Wang, J., Gao, Y., & Wang, L. (2016). Commutation analysis of brushless DC motor and reducing commutation torque ripple in the two-phase stationary frame. *IEEE Transactions on Power Electronics*, *32*(6), 4675-4682. https://doi.org/10.1109/TPEL.2016.2604422

Kommula, B. N., & Kota, V. R. (2022). An integrated converter topology for torque ripple minimization in BLDC motor using an ITSA technique. *Journal of Ambient Intelligence and Humanized Computing*, *13*(4), 2289-2308. https://doi.org/10.1007/s12652-021-02986-4

Kumar, R., & Singh, B. (2017). Solar PV powered BLDC motor drive for water pumping using Cuk converter. *IET Electric Power Applications*, *11*(2), 222-232. https://doi.org/10.1049/iet epa.2016.0328.

Li, Z., Kong, Q., Cheng, S., & Liu, J. (2020). Torque ripple suppression of brushless DC motor drives using an alternating two-phase and three-phase conduction mode. *IET Power Electronics*, *13*(8), 1622-1629. https://doi.org/10.1049/iet-pel.2019.0960.

Lu, H., Zhang, L., & Qu, W. (2008). A new torque control method for torque ripple minimization of BLDC motors with un-ideal back EMF. *IEEE transactions on power electronics*, *23*(2), 950-958. https://doi.org/10.1109/TPEL.2007.915667

Masmoudi, M., El Badsi, B., & Masmoudi, A. (2014). Direct torque control of brushless DC motor drives with improved reliability. *IEEE Transactions on Industry Applications*, *50*(6), 3744-53. https://doi.org/10.1109/TIA.2014.2313700

Niapour, S. K., Tabarraie, M., & Feyzi, M. R. (2014). A new robust speed-sensorless control strategy for high-performance brushless DC motor drives with reduced torque ripple. *Control Engineering Practice*, 24, 42-54. https://doi.org/10.1016/j.conengprac.2013.11.014.

Nithin, K. S., Vivek, R. S., & Purushothaman, A. (2020, November). Commutation Torque Ripple Comparison in Cuk Converter Fed Brushless DC Motor Drives with Mode Switching Selection Circuit. In *2020 International Conference on Power Electronics and Renewable Energy Applications (PEREA)* (pp. 1-6). IEEE. https://doi.org/10.1109/PEREA51218.2020.9339770

Park, J., & Lee, D. H. (2020). Simple commutation torque ripple reduction using PWM with compensation voltage. *IEEE Transactions on Industry Applications*, *56*(3), 2654-2662. https://doi.org/10.1109/TIA.2020.2968412

Park, S. J., Park, H. W., Lee, M. H., & Harashima, F. (2000). A new approach for minimum-torque-ripple maximum-efficiency control of BLDC motor. *IEEE Transactions on industrial electronics*, *47*(1), 109-114. https://doi.org/10.1109/41.824132

Patel, H., & Chandwani, H. (2021). Simulation and experimental verification of modified sinusoidal pulse width modulation technique for torque ripple attenuation in Brushless DC motor drive. *Engineering Science and Technology, an International Journal*, *24*(3), 671-681. https://doi.org/10.1016/j.jestch.2020.11.003

Periasamy, M., & Umaya, C. (2018). Improved Time Responses of PI & FL Controlled SEPIC Converter based Series Resonant Inverter-fed Induction Heating System. *International Journal of Power Electronics and Drive System (IJPEDS*), *9*(1), 305-315. https://doi.org/10.11591/ijpeds.v9.i1.pp305-315

Poorali, B., Adib, E., & Farzanehfard, H. (2017). Soft-switching DC–DC Cuk converter operating in discontinuous-capacitor-voltage mode. *IET Power Electronics*, *10*(13), 1679-1686. https://doi.org/10.1049/iet-pel.2016.0513

Rajesh, P., Shajin, F. H., & Cherukupalli, K. (2021). An efficient hybrid tunicate swarm algorithm and radial basis function searching technique for maximum power point tracking in wind energy conversion system. *Journal of Engineering, Design and Technology*. Vol. ahead-of-print No. ahead-of-print. https://doi.org/10.1108/JEDT-12-2020-0494

Rajesh, P., Shajin, F. H., & VijayaAnand, N. (2021). An efficient estimation model for induction motor using BMO-RBFNN technique. *Process Integration and Optimization for Sustainability*, *5*(4), 777-792. https://doi.org/10.1108/JEDT-12-2020-0494

Sadda, A., Keshri, J. P., Tiwari, H., & Jain, V. (2022). BLDC Motor Torque Ripple Minimization Technique by Using Isolated Type DC–DC Buck–Boost Converter. In *Advances in Energy Technology* (pp. 301-312). Springer, Singapore. https://doi.org/10.1007/978-981-16-1476-7_29

Senthilnathan, A., & Palanivel, P. (2020). A new approach for commutation torque ripple reduction of FPGA based brushless DC motor with outgoing phase current control. *Microprocessors and Microsystems*, *75*, Article 103043. https://doi.org/10.1016/j.micpro.2020.103043

Seol, H. S., Kang, D. W., Jun, H. W., Lim, J., & Lee, J. (2017). Design of winding changeable BLDC motor considering demagnetization in winding change section. IEEE Transactions on Magnetics, 53(11), 1-5. https://doi.org/10.1109/TMAG.2017.2695890

Shajin, F. H., & Rajesh, P. (2022). FPGA realization of a reversible data hiding scheme for 5G MIMO OFDM system by chaotic key generation-based paillier cryptography along with LDPC and its side channel estimation using machine learning technique. *Journal of Circuits, Systems and Computers*, *31*(05), 2250093. https://doi.org/10.1142/S0218126622500931

Shajin, F. H., Rajesh, P., & Raja, M. R. (2022). An efficient VLSI architecture for fast motion estimation exploiting zero motion prejudgment technique and a new quadrant-based search algorithm in HEVC. *Circuits, Systems, and Signal Processing*, *41*(3), 1751-1774. https://doi.org/10.1007/s00034-021-01850-2

Sheng, T., Wang, X., Zhang, J., & Deng, Z. (2014). Torque-ripple mitigation for brushless DC machine drive system using one-cycle average torque control. *IEEE Transactions on Industrial Electronics, 62*(4), 2114-2122. https://doi.org/10.1109/TIE.2014.2351377

Shi, T., Cao, Y., Jiang G., Li, X., & Xia, C. (2017). A torque control strategy for torque ripple reduction of brushless DC motor with nonideal back electromotive force. *IEEE Transactions on Industrial Electronics*, *64*(6), 4423-4433. https://doi.org/10.1109/TIE.2017.2674587

Shi, T., Guo, Y., Song, P., & Xia, C. (2009). A new approach of minimizing commutation torque ripple for brushless DC motor based on DC–DC converter. *IEEE Transactions on industrial electronics*, *57*(10), 3483-3490. https://doi.org/10.1109/TIE.2009.2038335

Shi, T., Niu, X., Chen, W., & Xia, C. (2017). Commutation torque ripple reduction of brushless DC motor in braking operation. *IEEE Transactions on Power Electronics*, *33*(2), 1463-1475. https://doi.org/10.1109/TPEL.2017.2675444

Singh, S., & Singh, B. (2012). A voltage-controlled PFC Cuk converter-based PMBLDCM drive for air conditioners. *IEEE transactions on industry applications*, *48*(2), 832-838. https://doi.org/10.1109/TIA.2011.2182329

Transpire Online. (2020). A Novel Numerical Optimization Algorithm Inspired from Particles: Particle Swarm Optimization. *Transpire Online*, 2020. Retrieved from https://transpireonline.blog/2019/07/03/a-novel-numerical-optimization-algorithm-inspired-from particles-particle-swarm-optimization/

Zhu, C., Zeng, Z., & Zhao R. (2016). Comprehensive analysis and reduction of torque ripples in three-phase four-switch inverter-fed PMSM drives using space vector pulse-width modulation. *IEEE transactions on power electronics*, *32*(7), 5411-5424. https://doi.org/10.1109/TPEL.2016.2605160